Peculiarities of the band structure of multi-component photonic crystals with different dimensions

2010 J. Phys.: Condens. Matter 22 115401

(http://iopscience.iop.org/0953-8984/22/11/115401)

IOP Publishing Journal of Physics: Condensed Matter

J. Phys.: Condens. Matter **22** (2010) 115401 (6pp) doi:10.1088/0953-8984/22/11/115401

Peculiarities of the band structure of multi-component photonic crystals with different dimensions

A K Samusev, K B Samusev, M V Rybin and M F Limonov

Ioffe Physical-Technical Institute of the Russian Academy of Sciences, St Petersburg 194021, Russia

E-mail: m.rybin@mail.ioffe.ru

Received 25 November 2009, in final form 11 January 2010
Published 23 February 2010
Online at stacks.iop.org/JPhysCM/22/115401

Abstract

In this work we offer a simple analytical method which allows us to determine and study the effects of the selective switching of photonic stop-bands in multi-component photonic crystals (Mc-PhCs) of any dimensionality. The calculations for Mc-PhCs with low dielectric contrast have been performed in the framework of the model based on the scattering form factor analysis. It has been shown that the effects of selective switching of photonic stop-bands predicted theoretically and found experimentally before in three-dimensional (3D) Mc-PhC have a general character and may be observed also in one-dimensional (1D) and two-dimensional (2D) Mc-PhCs. It is found that 1D, 2D and 3D Mc-PhCs demonstrate unexpectedly similar quasi-periodic behaviour of photonic stop-bands as a function of the reciprocal lattice vector. A proper choice of the structural and dielectric parameters can create a resonance photonic stop-band determining the Bragg wavelengths, to which a photonic crystal can never be transparent.

(Some figures in this article are in colour only in the electronic version)

1. Introduction

The architecture of a photonic crystal (PhC) is somewhat similar to that of computer architecture, which defines the way in which a central processing unit performs internally and interacts with other components. A PhC, which in our view can be considered to be analogous to a central processing unit, should ideally be designed to manipulate the flow of photons as effectively as a central processing unit (or possibly any electronic device) manipulates the flow of electrons or holes.

When considering the conceptual design and operational structure of a PhC one should select the shape and dielectric properties of the photonic building blocks and their distribution in space. Here we should note that in most theoretical and experimental studies PhCs have been considered as two-component structures, consisting of a periodic array of two homogeneous materials having different dielectric permittivity constants [1–3]. All the photonic stop-bands in such PhCs disappear simultaneously when the permittivities of the two materials (two components) become equal. Independent control over the selective switching of stop-bands in such PhCs is impossible. Multi-component PhCs (Mc-PhCs), which we define as periodic structures consisting of three or more homogeneous components (or when at least one of the components is inhomogeneous), have received much less attention. We can mention only a few papers that have considered PhCs with more than two components [4–10]. Systematic studies of Mc-PhCs were conducted on 3D PhC structures in [11, 12]. It has been experimentally demonstrated that Mc-PhCs possess qualitatively new photonic properties, which well-studied two-component PhCs do not exhibit. Specifically, Mc-PhCs demonstrate (i) the existence of the resonance stop-bands, which cannot be switched-OFF; (ii) selective switching of a specific stop-band (i.e. selective ON/OFF switching). These properties allow one to consider the possibility to selectively control the light propagation at different wavelengths. Experimental results obtained on synthetic opals have been described in the framework of the analytical model. While the precision of the model decreases when the dielectric permittivity contrast exceeds certain limits, its practical use and further development appears quite promising. This model not only allows one to

calculate photonic properties of PhC with the known structural parameters ('direct problem'), but most importantly design the structure of a PhC with the desired optical properties ('inverse problem'). The solution of this problem by using numerical computation methods [4, 13–17] involves to a large extent a purely intuitive search [18].

In the present work, a detailed theoretical study of the photonic stop-band switching effects in Mc-PhCs of different dimensions has been carried out in an approach similar to [11, 12, 19]. Earlier this approach was successfully used to describe selective ON/OFF stop-band switching in classical PhCs, i.e. synthetic opals, that were previously considered as two-component structures [20–30]. It is also important to note that one should be careful in using the analytical approach in the case of high dielectric contrast as well as in the case of a multiple Bragg diffraction regime, i.e. when stop-bands corresponding to different wavevectors overlap. In this case, the non-diffraction condition should be obtained by solving the full eigenvalue problem using numerical methods.

2. The structure of Mc-PhCs with different dimensions

Figure 1 shows the architectural principles for constructing two-component and multi-component PhCs of different dimensions, used in our theoretical studies. The three-component PhC (3c-PhC) is the simplest example of an Mc-PhC and is also drawn in figure 1. In this work we consider 3c-PhCs with different dimensions as follows.

(i) The 1D 3c-PhC, composed of dielectric slabs of three sorts, which are closely packed along the coordinate axis, say, for generality with PhCs with other dimensions, r. Let us refer to these three components (slabs) as: (1) N (nucleus) with width $2r_n$ and permittivity constant ε_n, (2) C (coat) with parameters $r_c - r_n$ and ε_c and (3) F (filler) with permittivity ε_f. The slabs are arranged in the ordered sequence of . . . FCNCFCNCF . . ., i.e. each of the N slabs is neighboured with two C slabs and F slabs are placed between the CNC blocks.

(ii) The 2D 3c-PhC, formed by infinite two-component non-overlapped cylinders arranged in a triangular or a square lattice structure. Each cylinder consists of a homogeneous cylindrical nucleus (N) and a homogeneous coating layer (C). The parameters of the N are the cylinder radius r_n and the permittivity constant ε_n. The parameters of the C are the internal radius r_n, the external radius $r_c \geqslant r_n$ and the permittivity constant ε_c. The interstice space is filled by a homogeneous material (F, filler) with permittivity ε_f.

(iii) The 3D 3c-PhC, constructed of non-overlapped spheres, the centres of which coincide with sites of an fcc lattice. Each sphere consists of the homogeneous nucleus (N) of the radius r_n and the permittivity ε_n and the homogeneous coating layer (C) surrounding the N and having an internal radius r_n, external radius $r_c \geqslant r_n$ and a permittivity constant ε_c. The interspherical space is filled by a homogeneous filling material (F) with permittivity ε_f.

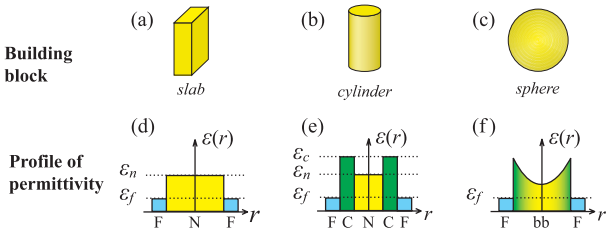

Figure 1. The conceptual design of PhCs. Simple examples of building blocks for PhCs with different dimensions (a)–(c). The permittivity distribution for two- (d) and multi-component (e), (f) structures.

Further, the F is considered in all three cases to be spatially homogeneous (ε_f = const). Let us refer to the two other structural elements (N and C) together as a 'building block'. For the 3c-PhC case, permittivities of N and C are constant. While for the general case of the Mc-PhC the permittivity value may vary within a building block boundary (figure 1).

(i) For the 1D Mc-PhC case the permittivity of the building block depends on the r coordinate value, $\varepsilon_n(r)$ and $\varepsilon_c(r)$ so it forms a symmetrical cell, i.e. $\varepsilon_n(r) = \varepsilon_n(-r)$, $\varepsilon_c(r) = \varepsilon_c(-r)$. Each building block is surrounded by the homogeneous filler ε_f = const.

(ii) For the 2D Mc-PhC case the permittivity of the building block has a radial symmetry of $\varepsilon_n(r)$ and $\varepsilon_c(r)$, where r is the radial coordinate.

(iii) For the 3D Mc-PhC case the permittivity of the building block has spherical symmetry of $\varepsilon_n(r)$ and $\varepsilon_c(r)$, where r is the radial coordinate as well.

All of the above-described Mc-PhCs with different dimensions will be considered further in the framework of the analytical approach to describe and calculate specific optical properties and the selective photonic stop-band switching conditions. The 3c-PhC case is of special interest because it provides a relatively easy analytical solution and representative results. In this work the photonic properties of Mc-PhCs have been studied depending on filler permittivity ε_f and, hence, we consider ε_f as a variable. Such variations can be realized in practice by changing the ε_f using some external means (such as electromagnetic field, temperature, mechanical stress etc) or simply by changing the filler material itself.

3. Mc-PhCs with arbitrary permittivity profile

The analytical model is based on a well-known fact: the Bragg diffraction from a set of crystal planes (characterized by Miller indices (h) for 1D, (hk) for 2D and (hkl) for 3D) underlies the existence of a corresponding (h) or (hk) or (hkl) stop-band. For this reason, in order to determine the conditions for the stop-band to arise and vanish, it is enough to consider the conditions for arising and vanishing of the Bragg diffraction from the specific set of the corresponding crystal planes. *The conditions of vanishing a particular stop-band will be referred to as 'OFF-switching conditions'.*

Let us consider the Fourier coefficient of the inverse of the permittivity, i.e. the scattering form factor $S(\mathbf{G})$:

$$S(\mathbf{G}) = \frac{1}{V_0}\int_{V_0} \mathrm{d}\mathbf{r}\,\frac{1}{\varepsilon(r)}\exp(-\mathrm{i}\mathbf{G}\cdot\mathbf{r}), \tag{1}$$

which describes the intensity of Bragg diffraction from a set of crystal planes as a function of the reciprocal lattice vector $\mathbf{G}$. The reciprocal lattice vector for 1D, 2D and 3D PhCs is $\mathbf{G}_h = h\mathbf{b}_1$, $\mathbf{G}_{hk} = h\mathbf{b}_1 + k\mathbf{b}_2$ and $\mathbf{G}_{hkl} = h\mathbf{b}_1 + k\mathbf{b}_2 + l\mathbf{b}_3$, respectively, where $\{\mathbf{b}_i; i = 1, 2, 3\}$ are the reciprocal lattice vectors. V_0 represents the length (1D PhC), area (2D PhC) or volume (3D PhC) of the Wigner–Seitz cell.

Consider a general case of an Mc-PhC with arbitrary dimensions (1D, 2D, 3D). The inverse permittivity of a Wigner–Seitz cell of the crystal is defined as

$$\frac{1}{\varepsilon(r)} = \frac{1}{\varepsilon_\mathrm{f}} + \left(\frac{1}{\varepsilon_{\mathrm{bb}}(r)} - \frac{1}{\varepsilon_\mathrm{f}}\right)\Theta(r_{\mathrm{bb}} - r), \tag{2}$$

where $\varepsilon_{\mathrm{bb}}(r)$ is an arbitrary profile of the permittivity of a building block possessing the proper (for the different dimensionality of 1D, 2D or 3D) symmetry described in section 2. The size of the building block is defined as $r_{\mathrm{bb}} = r_\mathrm{c}$. The unit step function is defined as: $\Theta(r) = 1$ at $r \geqslant 0$ and $\Theta(r) = 0$ at $r < 0$.

We will analyse the stop-band OFF-switching conditions, when the scattering form factor turns to zero $S(\mathbf{G}) = 0$. At $|\mathbf{G}| \neq 0$, the relation $S(\mathbf{G}) = 0$ can be rewritten as

$$S(\mathbf{G}) = \frac{1}{V_0}\int_{V_0} \mathrm{d}\mathbf{r}\left(\frac{1}{\varepsilon_{\mathrm{bb}}(r)} - \frac{1}{\varepsilon_\mathrm{f}}\right)\Theta(r_{\mathrm{bb}} - r)\exp(-\mathrm{i}\mathbf{G}\cdot\mathbf{r}) = 0. \tag{3}$$

As mentioned above, we take the filler to be the homogeneous material ($\varepsilon_\mathrm{f} = \mathrm{const}$). Therefore (3) gives the filler permittivity value yielding the *photonic stop-band OFF-switching condition* which is uniquely determined by the reciprocal lattice vector $\mathbf{G}$. Such a value of the filler permittivity will be denoted by $\varepsilon_\mathrm{f}^0(G)$, where $G = |\mathbf{G}|$. Integration of the appropriate expressions provides $\varepsilon_\mathrm{f}^0(G)$ for Mc-PhCs of different dimensionality:

For 1D Mc-PhC:
$$\varepsilon_\mathrm{f}^0(G) = \frac{\sin(G\,r_{\mathrm{bb}})}{G\int_0^{r_{\mathrm{bb}}}\frac{1}{\varepsilon_{\mathrm{bb}}(r)}\cos(Gr)\,\mathrm{d}r}. \tag{4a}$$

For 2D Mc-PhC:
$$\varepsilon_\mathrm{f}^0(G) = \frac{r_{\mathrm{bb}}J_1(Gr_{\mathrm{bb}})}{G\int_0^{r_{\mathrm{bb}}}\frac{1}{\varepsilon_{\mathrm{bb}}(r)}\,r\,J_0(Gr)\,\mathrm{d}r}. \tag{4b}$$

For 3D Mc-PhC:
$$\varepsilon_\mathrm{f}^0(G) = \frac{R(Gr_{\mathrm{bb}})}{G^2\int_0^{r_{\mathrm{bb}}}\frac{1}{\varepsilon_{\mathrm{bb}}(r)}\,r\sin(Gr)\,\mathrm{d}r}. \tag{4c}$$

In (4*b*) $J_0(x)$, $J_1(x)$ are the zeroth- and first-order Bessel functions of the first kind, while in (4*c*) $R(x) \equiv \sin(x) - x\cos(x)$ is the Rayleigh–Hans function.

To understand the behaviour of $\varepsilon_\mathrm{f}^0(G)$ as a function of the modulus of the reciprocal lattice vector, we do not limit the analysis to the discrete values of G (G_h in 1D, G_{hk} in 2D and G_{hkl} in 3D cases) but consider it as a continuous function G and omit the hkl indices.

4. Three-component photonic crystals

As a representative example, we consider the case of the stop-band OFF-switching conditions for the 3c-PhC of different dimensionality. In this case building blocks consist of a homogeneous nucleus and homogeneous coat. The formula (2) for the inverse permittivity of a Wigner–Seitz cell could be rewritten as:

$$\frac{1}{\varepsilon(r)} = \frac{1}{\varepsilon_\mathrm{f}} + \left(\frac{1}{\varepsilon_\mathrm{c}} - \frac{1}{\varepsilon_\mathrm{f}}\right)\Theta(r_\mathrm{c} - r) + \left(\frac{1}{\varepsilon_\mathrm{n}} - \frac{1}{\varepsilon_\mathrm{c}}\right)\Theta(r_\mathrm{n} - r). \tag{5}$$

The corresponding expressions for $\varepsilon_\mathrm{f}^0(G)$ now have the following form that is convenient for detailed analysis:

For 1D 3c-PhC:
$$\frac{1}{\varepsilon_\mathrm{f}^0} = \frac{1}{\varepsilon_\mathrm{c}} + \left(\frac{1}{\varepsilon_\mathrm{n}} - \frac{1}{\varepsilon_\mathrm{c}}\right)\frac{\sin(Gr_\mathrm{n})}{\sin(Gr_\mathrm{c})}. \tag{6a}$$

For 2D 3c-PhC:
$$\frac{1}{\varepsilon_\mathrm{f}^0} = \frac{1}{\varepsilon_\mathrm{c}} + \left(\frac{1}{\varepsilon_\mathrm{n}} - \frac{1}{\varepsilon_\mathrm{c}}\right)\frac{r_\mathrm{n}}{r_\mathrm{c}}\frac{J_1(Gr_\mathrm{n})}{J_1(Gr_\mathrm{c})}. \tag{6b}$$

For 3D 3c-PhC:
$$\frac{1}{\varepsilon_\mathrm{f}^0} = \frac{1}{\varepsilon_\mathrm{c}} + \left(\frac{1}{\varepsilon_\mathrm{n}} - \frac{1}{\varepsilon_\mathrm{c}}\right)\frac{R(Gr_\mathrm{n})}{R(Gr_\mathrm{c})}. \tag{6c}$$

As can be seen from (4*a*)–(4*c*) and (6*a*)–(6*c*), in any instance the ε_f^0 value, which determines the stop-band OFF-switching conditions, depends on the modulus of the reciprocal lattice vector G. So in an Mc-PhC of any dimension the selective photonic stop-band switching regime can take place.

5. The resonance stop-band in Mc-PhCs

Another important result follows at once from the formulae considered ((4*a*)–(4*c*) and (6*a*)–(6*c*)): the photonic stop-band OFF-switching condition has quasi-periodic character with the resonance features depending on G. By a resonance condition we imply such a value of $G = G_\mathrm{res}$ at which $\varepsilon_\mathrm{f}^0 \to \pm\infty$. Infinite permittivity is impossible, therefore the stop-band corresponding G_res cannot be switched-OFF by changing the filler permittivity, i.e. in this case OFF-switching condition is unfeasible. The expressions (4*a*)–(4*c*) and (6*a*)–(6*c*) point out that alternations of the sign of functions $\sin(Gr)$, $J_1(Gr)$ and $R(Gr)$ (see figure 2) are responsible for the resonance $\varepsilon_\mathrm{f}^0 \to \pm\infty$. Note that the resonant values $G = G_\mathrm{res}$ are determined by the following equations:

For 1D 3c-PhC:
$$\frac{1}{\varepsilon_\mathrm{c}} = \left(\frac{1}{\varepsilon_\mathrm{c}} - \frac{1}{\varepsilon_\mathrm{n}}\right)\frac{\sin(Gr_\mathrm{n})}{\sin(Gr_\mathrm{c})}. \tag{7a}$$

For 2D 3c-PhC:
$$\frac{1}{\varepsilon_\mathrm{c}} = \left(\frac{1}{\varepsilon_\mathrm{c}} - \frac{1}{\varepsilon_\mathrm{n}}\right)\frac{r_\mathrm{n}}{r_\mathrm{c}}\frac{J_1(Gr_\mathrm{n})}{J_1(Gr_\mathrm{c})}. \tag{7b}$$

For 3D 3c-PhC:
$$\frac{1}{\varepsilon_\mathrm{c}} = \left(\frac{1}{\varepsilon_\mathrm{c}} - \frac{1}{\varepsilon_\mathrm{n}}\right)\frac{R(Gr_\mathrm{n})}{R(Gr_\mathrm{c})}. \tag{7c}$$

6. Discussion

Let us discuss the stop-band OFF-switching conditions obtained above and compare it with the experimental data [11, 12]. Figure 3 shows $\varepsilon_\mathrm{f}^0(G)$ dependences determined

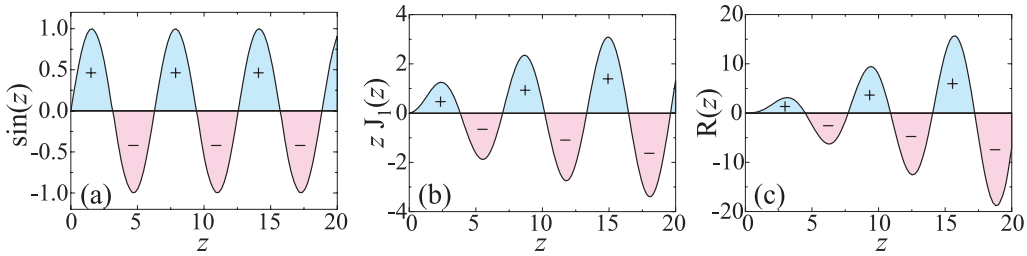

Figure 2. The graph of alternating-sign functions: (a) the sine function; (b) the first-order Bessel function of the first kind multiplied by its argument; (c) the Rayleigh–Hans function.

by (4*c*). The figure demonstrates characteristic $\varepsilon_f^0(G)$ function behaviour at the region of small G in its dependence on the dielectric parameters. In the trivial case of $\varepsilon_n = \varepsilon_c$ (i.e. reduction to the two-component PhC) equation (4*c*) gives the following solution $\varepsilon_f^0(G) = \varepsilon_n = \varepsilon_c$. This solution corresponds to the case of the optically homogeneous structure, therefore the OFF-switching conditions are fulfilled simultaneously for any stop-band, i.e. the transmission coefficient becomes unity (figure 4(g)). It is clear that the graph of the $\varepsilon_f^0(G)$ function corresponds to the horizontal line on figure 3. It worth noting that the $\varepsilon_f^0(G)$ function changes dramatically when the nucleolus to coat the dielectric contrast appears ($\varepsilon_n \neq \varepsilon_c$). Now there is no such filler permittivity value ε_f that makes the structure optically homogeneous. In this case $\varepsilon_f^0(G)$ dependences become quasi-periodical and resonant. When the nucleus is denser ($\varepsilon_n > \varepsilon_c$) the $\varepsilon_f^0(G)$ function increases, and when the coat is denser ($\varepsilon_n < \varepsilon_c$) the $\varepsilon_f^0(G)$ function decreases. Such a behaviour is specific for small values of $G \lesssim 30$, where the $\varepsilon_f^0(G)$ function is being inverted (figure 5).

In figure 3, in addition to the $\varepsilon_f^0(G)$ dependences calculated we present the experimental data from [12]. They were obtained in studies of the immersion dependences of the transmission spectra of the opal based PhC consisting of close-packed a-SiO_2 spheres. Here 'immersion dependence' means dependence of the transmission spectrum on the filler permittivity ε_f. In this experiment two liquids (namely, distilled water with $\varepsilon_w = 1.78$ and propylene glycol with $\varepsilon_{pg} = 2.05$) as well as their mixtures were used as an opal matrix filler providing the variation of its dielectric constant in the range of $1.78 \leqslant \varepsilon_f \leqslant 2.05$. The immersion behaviour of the following families of photonic band gaps has been revealed: {111}, {200}, {220}, {311} and {222}. As a result, it was shown that the stop-bands disappear (i.e. the OFF-switching condition is fulfilled) at very different values of the filler permittivity ε_f (figures 4(d) and (i)). Two values $\varepsilon_f^0(G_{111}) \sim 1.82$ and $\varepsilon_f^0(G_{220}) \sim 1.93$ were obtained directly from the measured data. In addition two other values $\varepsilon_f^0(G_{200}) \sim 1.63$ and $\varepsilon_f^0(G_{311}) \sim 1.75$ were obtained by extrapolating data out of the measured region ($1.78 \leqslant \varepsilon_f \leqslant 2.05$). Besides, it was shown that the {222} stop-band's dip intensity virtually does not depend on the filler permittivity ε_f (figure 4(j)). For this reason the {222} stop-band was attributed to be resonant. The experimentally obtained $\varepsilon_f^0(G_{hkl})$ values are presented in figure 3. The values of the moduli of the reciprocal lattice vector G_{hkl} for an fcc opal lattice are the following:

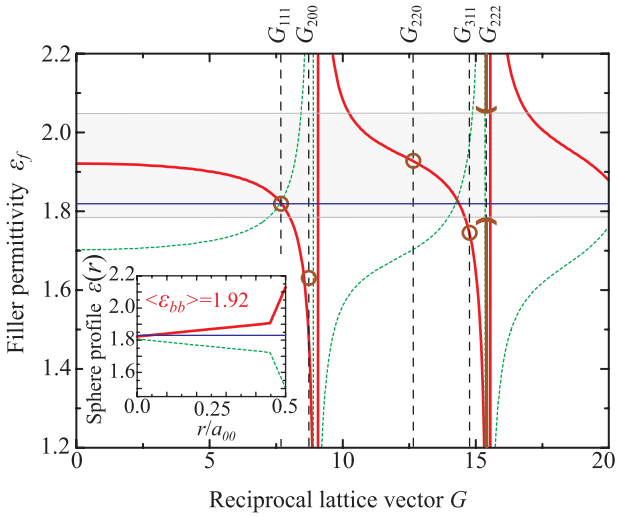

Figure 3. Non-diffraction conditions for an opal-like structure obtained from measured and extrapolated data from [12] (circles) and from calculations (curves). The filler permittivity $\varepsilon_f^0(G)$ as a function of the reciprocal lattice vector calculated from equation (4*c*) for the permittivity profile $\varepsilon_{bb}(r)$ simulating the a-SiO_2 spheres. The $\varepsilon_{bb}(r)$ profiles given in the inset and the corresponding filler permittivity $\varepsilon_f^0(G)$ are presented by the same curves (green dashed curves, blue thin lines, red thick curves). The grey region is for the experimental range of ε_f. The moduli of the shortest reciprocal lattice vector G_{hkl} are shown by vertical lines. The values of G are taken in the units of the reciprocal distance between centres of the nearest spheres a_{00}.

$G_{111} = 7.70$, $G_{200} = 8.89$, $G_{220} = 12.57$, $G_{311} = 14.74$, $G_{222} = 2$, $G_{111} = 15.40$. One can easily find them with use of the formula $G_{hkl} = \pi\sqrt{2(h^2 + k^2 + l^2)}a_{00}^{-1}$ (here the values of G_{hkl} are taken in the units of the reciprocal distance between centres of the nearest spheres a_{00}).

From figure 3 one can conclude unambiguously that in opal the a-SiO_2 spheres' coating layer is optically denser than the nucleus. This is approved especially by the results of scanning electron microscopy (SEM) and transmission electron microscopy (TEM) investigations [12]. Also note the theoretical prediction of a resonant feature close to $G_{222} = 15.40$ which is in good agreement with the {222} stop-band family behaviour observed experimentally.

Here we summarize the main conclusions following from the results presented in figure 4. In Mc-PhCs, which are optically inhomogeneous structures, simultaneous OFF switching for all of the stop-bands is impossible. However, for any given stop-band related to the G_{hkl} one can obtain the

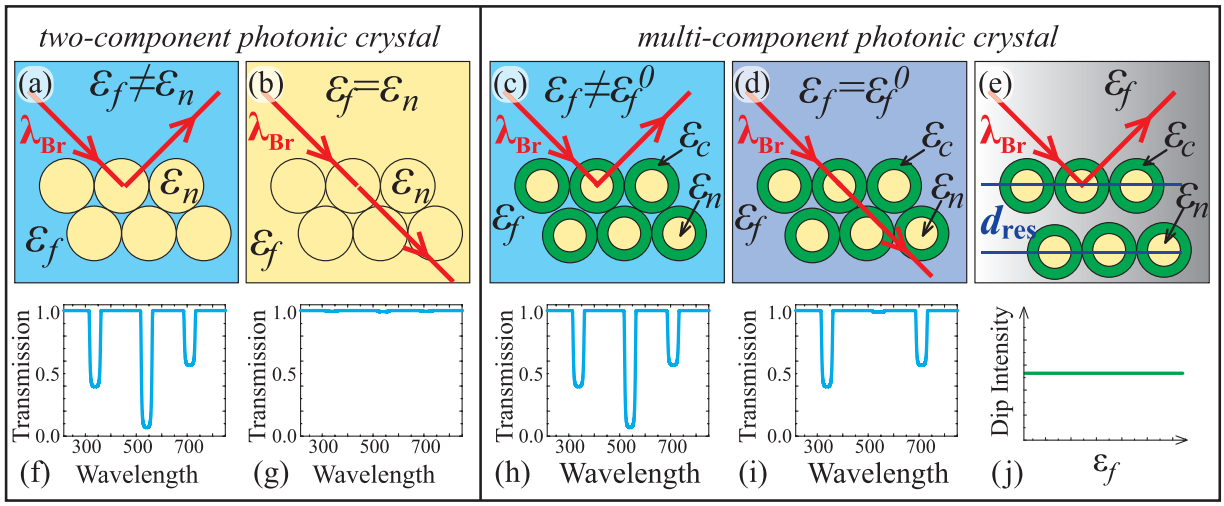

Figure 4. Schematic comparison of the Bragg diffraction by a two-component PhC and an Mc-PhC (upper panels) and corresponding transmission spectra (lower panels). For a two-component PhC: the general case of the Bragg scattering (a), (f) and the non-diffraction regime (b), (g). For an Mc-PhC: the general case of the Bragg scattering (c), (h), the non-diffraction selective regime (d), (i) and the resonant 'non-immersive' stop-bands (e), (j).

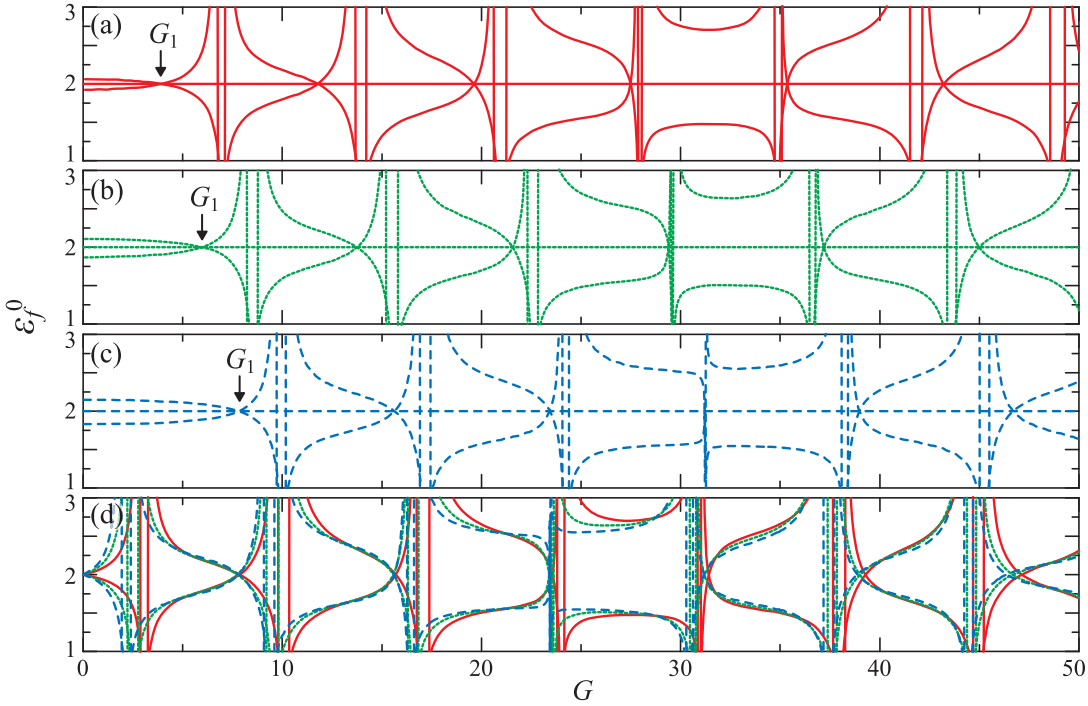

Figure 5. (a)–(c) The filler permittivity $\varepsilon_f^0(G)$ of a 3c-PhC in the non-diffraction regime as a function of the reciprocal lattice vector G, calculated from equations (6*a*)–(6*c*) for structures composed of building blocks with the nucleus of radius $r_n = 0.35$ ($\varepsilon_n = 2.0$) and different coats ($r_c = 0.45$, $\varepsilon_c = 1.7, 2.0, 2.3$) for different dimensions: (a) 1D—red solid, (b) 2D—green dotted and (c) 3D blue dashed. (d) The comparison of the $\varepsilon_f^0(G)$ dependences for three different dimensions. The curves are shifted by the value of the first root G_1 (shown by arrows). The styles of the curves correspond to (a)–(c).

OFF-switching condition using expression (4*c*) (figures 4(d) and (i)). This means the structure becomes transparent for the corresponding Bragg wavelengths. The exception is a resonant stop-band, the parameters of which are determined from formulae (7*a*)–(7*c*). The resonant stop-band could not be OFF-switched by varying ε_f (figure 4(j)).

One more property of the $\varepsilon_f^0(G)$ function is demonstrated in figure 5. The figure presents a wide range of G dependences of $\varepsilon_f^0(G)$ for 1D 3c-PhC (a), 2D 3c-PhC (b) and 3D 3c-PhC (c), which are plotted like the ones shown in figure 3, i.e. there are three cases considered $\varepsilon_n = \varepsilon_c$, $\varepsilon_n > \varepsilon_c$ and $\varepsilon_n < \varepsilon_c$. Now let us consider the specific feature of the $\varepsilon_f^0(G)$ function, namely, special quasi-periodic points at $G = G_n$, when all three curves intersect at the value $\varepsilon_f^0(G_n) = \varepsilon_n$. Indeed, from equations (6*a*)–(6*c*) one can obtain the G-coordinate of such a point. The corresponding values G_n determined with use of

equations (6*a*)–(6*c*) are:

$$\text{For 1D 3c-PhC:} \qquad \sin(Gr_n) = \sin(Gr_c). \tag{8a}$$

$$\text{For 2D 3c-PhC:} \qquad r_n J_1(Gr_n) = r_c J_1(Gr_c). \tag{8b}$$

$$\text{For 3D 3c-PhC:} \qquad R(Gr_n) = R(Gr_c). \tag{8c}$$

For example, at $r_n = 0.35$ and $r_c = 0.45$, the first root G_1 of equations (8*a*)–(8*c*) (i.e. the smallest G_n value) is $G_1 \approx 3.93$ (1D), 6.00 (2D), 7.81 (3D).

To analyse the influence of the geometrical dimensionality we have superposed curves from figures 5(a)–(c) onto 5(d). All the curves were shifted along the abscissas by G_1. A quite unexpected result is revealed by figure 5(d). In spite of the fact that OFF-switching conditions in 3c-PhC with different dimensions have different mathematical definitions (namely, using functions $\sin(x)$ for (1D), $J_1(x)$ for (2D), $R(x)$ for (3D)), after shifting by G_1 the functions $\varepsilon_f^0(G - G_1)$ virtually do not depend on the PhC dimensionality. The same result was obtained for the general case of Mc-PhCs.

7. Conclusion

In this work we have discussed an 'architectural' approach in studies of the structural and optical properties of the PhC. The base element forming the PhC structure and mainly determining its optical properties is its 'building block', which can be represented by a slab, cylinder, sphere etc. The permittivity profile $\varepsilon_{bb}(r)$, which classifies a PhC as a two-component PhC ($\varepsilon_{bb} = \text{const}$) and an Mc-PhC and plays the key role in photonic band gap structure formation, is a general characteristic of the building block. The Mc-PhC is formed from building blocks with an inhomogeneous permittivity profile $\varepsilon_{bb}(r)$ and, hence, its structure is optically inhomogeneous irrespective of the filler permittivity ε_f. We have discussed in detail the problem of optical transparency of such an inhomogeneous Mc-PhC. It has been shown that for a given stop-band one could fulfil the OFF-switching condition using the appropriate filler permittivity $\varepsilon_f^0(G)$. This means the Mc-PhC becomes transparent at the corresponding Bragg wavelengths. The only exception is the resonant 'non-immersive' stop-bands, i.e. stop-bands that cannot be switched-OFF by varying the permittivity of one of the components. Resonant stop-bands determine the Bragg wavelengths at which the Mc-PhC is opaque. The described photonic properties are immanent to Mc-PhCs of any dimension (1D, 2D and 3D).

It is noteworthy that the quantitative results obtained in this study are applicable to the low dielectric contrast case only. However, we believe the general ideas on which the analytical approach is based possess the necessary generality to be adapted to the case of high dielectric contrast PhC structures.

Acknowledgments

We thank G Yushin, A B Khanikaev, A V Baryshev and A A Kaplyanskii for fruitful discussions. This work was supported by the RFBR, grant 08-02-00642 and by the Government of Saint Petersburg, Russia.

References

[1] Joannopoulos J D, Johnson S G, Winn J N and Meade R D 2008 *Photonic Crystals: Molding the Flow of Light* 2nd edn (Princeton, NJ: Princeton University Press) p 304
[2] Inoue K and Ohtaka K (ed) 2004 *Photonic Crystals: Physics, Fabrication and Applications* (Berlin: Springer) p 348
[3] Sakoda K 2004 *Optical Properties of Photonic Crystals* 2nd edn (Berlin: Springer) p 272
[4] Sözüer H, Haus J and Inguva R 1992 *Phys. Rev.* B **45** 13962–72
[5] Velikov K P, Moroz A and van Blaaderen A 2002 *Appl. Phys. Lett.* **80** 49–51
[6] Takeda H and Yoshino K 2002 *Appl. Phys. Lett.* **80** 4495–7
[7] Takeda H and Yoshino K 2003 *J. Appl. Phys.* **93** 3188–93
[8] Galisteo-López J, García-Santamaría F, Golmayo D, Juárez B, López C and Palacios-Lidón E 2004 *Photon. Nanostruct.: Fundam. Appl.* **2** 117–25
[9] García P D, Galisteo-López J F and López C 2005 *Appl. Phys. Lett.* **87** 201109
[10] Glushko A and Karachevtseva L 2006 *Photon. Nanostruct.: Fundam. Appl.* **4** 141–5
[11] Baryshev A, Khanikaev A, Inoue M, Lim P, Selkin A, Yushin G and Limonov M 2007 *Phys. Rev. Lett.* **99** 063906
[12] Rybin M V, Baryshev A V, Khanikaev A B, Inoue M, Samusev K B, Sel'kin A V, Yushin G and Limonov M F 2008 *Phys. Rev.* B **77** 205106
[13] Ho K M, Chan C T and Soukoulis C M 1990 *Phys. Rev. Lett.* **65** 3152–5
[14] Busch K and John S 1998 *Phys. Rev.* E **58** 3896–908
[15] Modinos A, Stefanou N, Psarobas I E and Yannopapas V 2001 *Physica* B **296** 167–73
[16] Pendry J B and MacKinnon A 1992 *Phys. Rev. Lett.* **69** 2772–5
[17] Kunz K and Luebbers R 1993 *The Finite Difference Time Domain Method for Electromagnetics* (Boca Raton, FL: CRC Press) p 459
[18] Burger M, Osher S and Yablonovitch E 2003 *IEICE Trans. Electron.* **87** 258–65
[19] Samusev A, Rybin M and Limonov M 2009 *Phys. Solid State* **51** 518–24
[20] Astratov V N, Bogomolov V N, Kaplyanskii A A, Prokofiev A V, Samoilovich L A, Samoilovich S M and Vlasov Y A 1995 *Nuovo Cimento* D **17** 1349–54
[21] Vlasov Y A, Astratov V N, Karimov O Z, Kaplyanskii A A, Bogomolov V N and Prokofiev A V 1997 *Phys. Rev.* B **55** R13357–60
[22] Míguez H, López C, Meseguer F, Blanco A, Vázquez L, Mayoral R, Ocana M, Fornés V and Mifsud A 1997 *Appl. Phys. Lett.* **71** 1148–50
[23] van Driel H M and Vos W L 2000 *Phys. Rev.* B **62** 9872–5
[24] Mazurenko D, Kerst R, Dijkhuis J, Akimov A V, Golubev V G, Kurdyukov D A, Pevtsov A B and Selkin A V 2003 *Phys. Rev. Lett.* **91** 213903
[25] Kaplan S, Kartenko N, Kurdyukov D, Medvedev A, Badalyan A and Golubev V 2007 *Photon. Nanostruct. Fundam. Appl.* **5** 37–43
[26] Baryshev A V, Kaplyanskii A A, Kosobukin V A, Samusev K B, Usvyat D E and Limonov M F 2004 *Phys. Rev.* B **70** 113104
[27] Baryshev A V, Khanikaev A B, Uchida H, Inoue M and Limonov M F 2006 *Phys. Rev.* B **73** 033103
[28] Rybin M V, Baryshev A V, Inoue M, Kaplyanskii A A, Kosobukin V A, Limonov M F, Samusev A K and Selkin A V 2006 *Phot. Nanost. Fund. Appl.* **4** 146–54
[29] Baryshev A, Kosobukin V, Samusev K, Usvyat D and Limonov M 2006 *Phys. Rev.* B **73** 205118
[30] Rybin M, Samusev K and Limonov M 2007 *Photon. Nanostruct.: Fundam. Appl.* **5** 119–24